Journal of the European Ceramic Society 20 (2000) 2079–2094

Influence of a crack on the electrical impedance of polycrystalline ceramics

A. Tiefenbach, B. Hoffmann *

Institut für Werkstoffe der Elektrotechnik (IWE), Universität Karlsruhe (TH), Adenauerring 20, D-76131 Karlsruhe, Germany

Received 29 September 1999; received in revised form 15 March 2000; accepted 25 March 2000

Abstract

The influence of a crack on the electrical impedance of single- and two-phase microstructures was investigated on zirconia ceramics experimentally by impedance spectroscopy and theoretically by extending the brick layer model. Accordingly a crack in a polycrystalline ceramic in general doubles the number of electrical time constants in the impedance spectra compared to the initial state. For single-phase materials this was experimentally proved on yttria stabilized specimens. However, in the case of realistic two-phase microstructures the spectra of the flawed materials are mostly characterized by two time constants as in the initial state. This also follows from the model and was found for ceria stabilized zirconia. Changes due to a crack always occur in the low-frequency range of the spectra. By means of the extended model and numerical field computations the qualitative and quantitative effects of a crack can clearly be reproduced. Consequently, the influence of a crack of any size on the electrical impedance can be predicted.

Keywords: Cracks; Impedance spectroscopy; ZrO_2

1. Introduction

For characterizing the electrical properties of polycrystalline ceramics impedance spectroscopy has often been used.[1–5] There is, however, only little information about impedance measurements on ceramic materials with defects such as cracks.

A new modelling is required to find a realistic description for the electrical properties of such a material. For the flawless state of a two-phase microstructure two models are often applied: The brick layer model treats the microstructure as an array of cubic-shaped grains.[6–8] This model assumes a continuous grain boundary phase separating the individual grains. In the case of low-conducting grain boundaries the electrical behaviour can be described by an equivalent circuit consisting of two R-C elements in series. If the coverage of the grains is not complete the ionic current can be divided into two paths, one of which is blocked capacitively, while the other is not.[9] The regions where good intergranular contact is established are called easy paths. The easy path model may especially be preferable if the coverage of the grains is low.

Both models can be used for flawless materials. The easy path model can also treat the influence of defects such as cracks.[10,11] However, the quantitative effects of the crack geometry are not considered. Furthermore, no model is known for the case of a microstructure where the coverage of the grains is complete and no intergranular contacts exist. Therefore, an as universal as possible description has to be developed from which the influence of a crack follows quantitatively.

The aim of the present work was to study the influence of an individual crack on the electrical impedance of two- as well as single-phase microstructures. For the experimental investigations Ce- and Y-stabilized zirconia were used. The theoretical investigations are based on a new model and numerical field computations.

2. Experimental procedure

ZrO_2-powders containing 9 mol% CeO_2 (9Ce-TZP, Unitec, UK), 2 mol% Y_2O_3 (2Y-TZP, Tosoh, Japan) and 8 mol% Y_2O_3 (8YSZ, Tosoh) were used as starting materials. The powders were compacted into plates by axial pre-compacting and subsequent cold isostatic pressing at 400–600 MPa. Sintering was carried out in air at 1400°C for 2 h in the case of 9Ce-TZP, at 1450°C

* Corresponding author. Fax: +49-721-608-7492.

0955-2219/00/$ - see front matter
PII: S0955-2219(00)00104-7

for 2.5 h in the case of 2Y-TZP and at 1600°C for 3 h in the case of 8YSZ. The heating and cooling rates were 2 K/min. The required specimen shapes were manufactured from the plates by diamond cutting and grinding. All specimens were annealed at 1200°C for 1 h to remove the monoclinic zone at the surface, induced by grinding.

The sample preparation and the microstructural characterization using TEM investigations were performed at the "Institut für Keramik im Maschinenbau" of the University of Karlsruhe.

The electrodes for the specimens were prepared by vacuum deposition of platinum. The electrical measurements were carried out over a temperature range from 300 to 500°C using an impedance analyser (SI 1260, Solartron) over a frequency range from 1 Hz to 1 MHz. In this case the measuring accuracy is 0.2%. The specimens were heated by high-intensity infra-red line heaters. All experiments were performed in air. The specimen size was $10\times8\times12$ mm^3.

The damage of the samples occurred by introducing an individual crack of perceptible crack length. On account of the specimen geometry at first a small indent was sawed into the sample. A stable crack could then be inserted mechanically using the bridge method and also be propagated successively as shown in Fig. 1. The impedance measurements were carried out on specimens with a crack running parallel to the electrodes in the middle of the specimen. Consequently, the electrical field is normally to the crack and one achieves a maximum measuring effect.

3. Experimental results

Impedance spectra were recorded firstly in the initial state and secondly after introducing individual cracks of different lengths in the specimens. For all materials porosities less than 0.5% were found in the initial state.

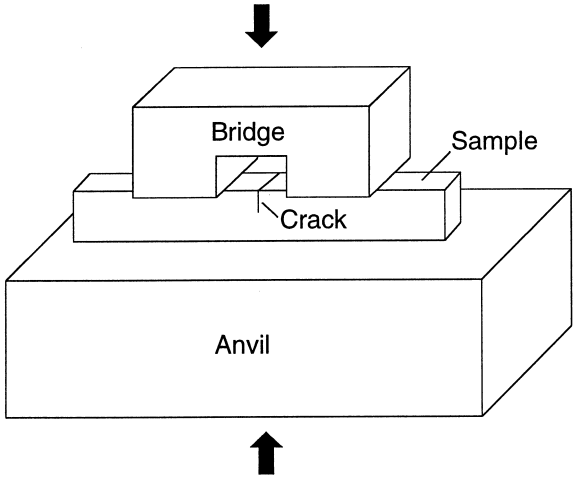

Fig. 1. Bridge method.

3.1. Electrical impedance of Ce-TZP

In the case of 9Ce-TZP, a two-phase microstructure with purely tetragonal grains was found. TEM investigations inclusive EDX analyses show that the grains are completely covered by a grain boundary phase.

The spectra of the specimens with only one crack are as in their flawless state characterized by two time constants, as shown in Fig. 2. In the high-frequency range there are no changes compared to the initial state. The crack electrically has its effect in the low-frequency range only. The resulting changes in the electrical properties can be observed as differences in the capacitive and resistive parts of the impedance. In particular the magnitude of the impedance of the ohmic range increases clearly with increasing crack length a_x.

3.2. Electrical impedance of yttria-stabilized zirconia

The 2Y-TZP exhibits a two-phase microstructure. This material is purely tetragonal. In the case of 8YSZ the crystal structure is purely cubic and a grain boundary phase could not be detected.

Since the stabilizer content in the initial state leads to clear and in particular qualitative differences in the spectra, as shown in Fig. 3, here, the influence of a crack

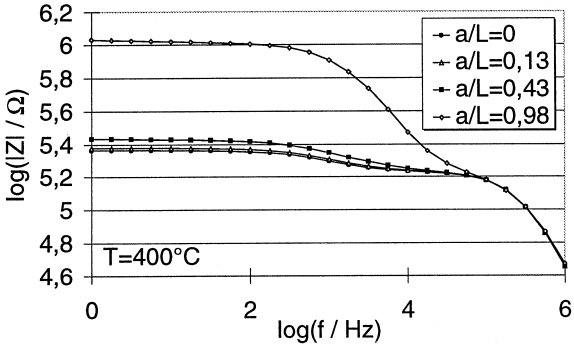

Fig. 2. Bode characteristics recorded at 400°C on a 9Ce-TZP specimen in the initial state and with individual cracks of different lengths.

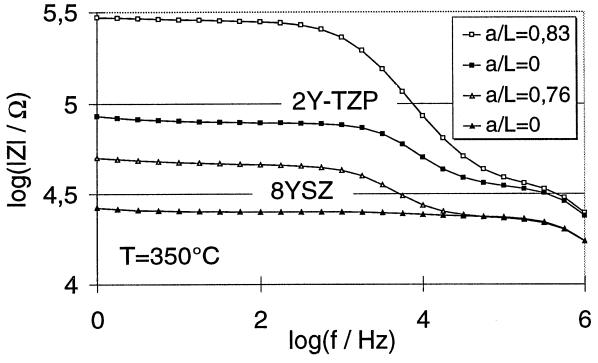

Fig. 3. Bode characteristics recorded at 350°C on yttria-stabilized specimens in the initial state and with an individual crack.

on the electrical impedance was of special interest. In the initial state 2Y-TZP electrically looks very similar to 9Ce-TZP. The spectra are also characterized by two time constants. However, only one time constant appears in the spectra in the case of 8YSZ.

For both Y-stabilized materials a multiple crack prolongation was not possible because of their very brittle behaviour. The first crack already extended over most of the sample cross section. In 8YSZ it was very difficult to introduce a crack into the sample without completely destroying it.

For 2Y-TZP, one also qualitatively finds the same electrical behaviour in the flawed state as for 9Ce-TZP. In the case of 8YSZ from the inserted crack results a second time constant, which appears in the low-frequency range of the impedance spectra and is clearly indicated by an additional ohmic and capacitive range. Such an additional contribution has been also found for simple contacts and different weldings between single crystals of a similar composition.[11] Moreover, this behaviour can be explained by the newly developed model which is the subject of the following section.

4. Theoretical results

Modelling was developed for an individual crack in a two-phase microstructure in the case of grains (index gi) completely covered by a grain boundary phase (index gb) as well as for a single-phase material. Compared to the conductivity in the grain boundary phases highly conducting grains are only considered: $\sigma_{gi} >> \sigma_{gb}$. Phase transformations do not occur over the temperature range used and therefore, have not to be considered.

4.1. Crack extended brick layer model

The crack damage inserted into the microstructure represents an additional, third phase and can be regarded as a very thin, air-filled, cavity (index A) with an electrical conductivity $\sigma_A = 0$ and a relative permittivity $\varepsilon_A = 1$. Qualitatively, the impedance spectra for the flawed material however, are, as in the initial state, electrically characterized by two time constants. In this respect a simulation of the electrical behaviour is displayed using an equivalent circuit, consisting of two R-C elements in series. However, the brick layer model in its simple form must not be applied in particular for physical reasons.

Therefore, the brick layer model was extended. In this paper, modelling was limited to an individual crack. A transfer of this model to several cracks might be possible.[12] The crack is integrated into the microstructure as an air-filled rectangular parallelepiped, as suggested in Fig. 4. It is defined by the crack opening δ_y, the length

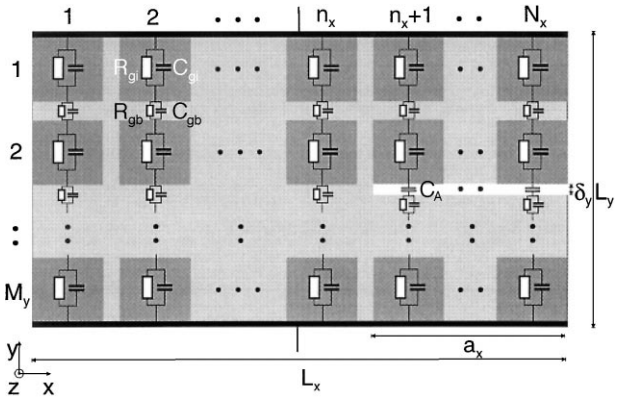

Fig. 4. Crack extended brick layer model and corresponding equivalent circuit.

a_x and is extended in z-direction along the whole sample length.

The sample contains N_x grains and grain boundary phases in x-direction, M_y in y-direction and K_z in z-direction. The crack length as well as the sample geometry might be expressed as a function of the mean grain size d_{gi} given by $a_x = (N_x - n_x)d_{gi}$ and $L_x = N_x d_{gi}$, $L_y = M_y d_{gi}$.

Although the crack represents a strongly localized damage, the current flow is assumed one-dimensional and normally to the electrodes. In this way, an analytical calculation of the total impedance becomes possible in a general form. In reality of course, current flow along the crack borders parallel to the electrodes and in bent lines around the crack tip occurs. This fact is considered later by means of the numerical field computations and the necessary corrections are carried out on the crack extended model. In the flawless regions current flow takes place through the grains and across the grain boundary phases. However, no ionic dc current flow is possible via the crack. There only a capacitive displacement current occurs. For a crack element of the length d_{gi}, the opening δ_y and with the angular frequency ω one obtains the impedance

$$Z_A = -j\frac{1}{\omega C_A} \text{ in which } C_A = \varepsilon_0 \frac{d_{gi}^2}{\delta_y}. \quad (1)$$

Assuming the electrodes parallel to the xz-plane uninterrupted current flow takes place in every xy-plane within the sample on n_x paths from one electrode to the other. Hence, the resulting impedance of a path in a flawless region (index Ref) is:

$$Z_{Path,Ref} = M_y\left(Z_{gi} + Z_{gb}\right) \quad (2)$$

in which

$$Z_i = \frac{R_i}{1 + (\omega R_i C_i)^2} - j\frac{\omega R_i^2 C_i}{1 + (\omega R_i C_i)^2}, \quad (3)$$

for $i = gi$, $i = gb$ and

$$R_i = \frac{r_i}{d_{gi}} = \frac{1}{\sigma_i}\frac{d_i}{d_{gi}^2},\ C_i = c_i d_{gi} = \varepsilon_0 \varepsilon_i \frac{d_{gi}^2}{d_i}. \quad (4)$$

On the residual $(N_x - n_x)$ paths, which is the flawed region, the impedance of a crack element according to Eq. (1) has to be added in each case, and one obtains for the path impedance

$$Z_{Path,Crack} = M_y\left(Z_{gi} + Z_{gb}\right) + Z_A. \quad (5)$$

From the shunt connection of all path impedances of a plane and finally of all planes impedances results the sample impedance for the flawed sample given by

$$Z_S = \frac{M_y^2\left(Z_{gi} + Z_{gb}\right)^2 + M_y\left(Z_{gi} + Z_{gb}\right)Z_A}{K_Z\left(N_x M_y\left(Z_{gi} + Z_{gb}\right) + n_x Z_A\right)}. \quad (6)$$

Unlike in the case of the brick layer model for flawless materials, here a geometry independent representation is not possible since the size of the crack plays an important role with respect to the sample geometry.

The corresponding electrical equivalent circuit can be found in Fig. 4.

4.2. Crack extended brick model

In the case of a flawless single-phase microstructure, only one time constant appears in the impedance spectra, as it was found for 8YSZ, and simply one R-C element is enough for a simulation. This R-C element represents the electrical behaviour of the grains and a grain boundary phase does not exist. Such a modelling shall be designated in the following as the brick model in contrast to the brick layer model.

Transmitting the results derived above for the crack extended brick layer model, the sample impedance for single-phase materials in the flawed state follows from Eq. (6) with $Z_{gb} = 0$ given by

$$Z_S = \frac{M_y}{N_x K_z}\frac{M_y Z_{gi}^2 + Z_{gi} Z_A}{M_y Z_{gi} + \frac{n_x}{N_x} Z_A}. \quad (7)$$

The corresponding equivalent circuit results from that in Fig. 4 if one disregards all the R-C elements which describe the grain boundary phases or instead of this bridges them.

4.3. Typical impedance spectra resulting from the crack extended models

The influence of a crack on the impedance given by Eqs. (6) and (7) is at this point considered by means of calculated spectra using the two crack extended models with a definite crack opening of $\delta_y = 2$ μm and for different crack lengths. This is compared with the spectra of the corresponding flawless states, which are determined by the brick model and the brick layer model. Typical values for the electrical properties of the phases of polycrystalline ceramics were used for the calculations. Fig. 5 shows all the characteristics.

If cracking occurs, both, for one- and for two-phase microstructures the curves are each characterized by two ohmic and two capacitive ranges. The influence of the crack particularly appears in an increasing magnitude of the low-frequency ohmic range.

In order to be able to calculate the influence of a crack from measured spectra a simplification of the equivalent circuits of the crack extended models is necessary. Nevertheless from the quantities of the remaining elements, the influences of the microstructure and of the crack damage must clearly result.

4.4. Simplified crack extended brick model

As shown before, typical impedance spectra for single-phase microstructures are characterized by two time constants when cracking occurs. Therefore in the case of single-phase microstructures, qualitatively a different electrical behaviour as in the flawless state has to be considered which can be represented by a network consisting of two R-C elements in series. Eq. (7) can be transformed into:[12]

$$Z_S = \frac{A_3\omega^3 + A_2\omega^2 + A_1\omega + A_0}{B_4\omega^4 + B_2\omega^2 + B_0}. \quad (8)$$

Then the facts become clear because the function of the total impedance of two R-C elements in series can be brought into the same form as Eq. (8) and hence is mathematically equivalent to the transfer function resulting from Eq. (7).[12] One can now compare the coefficients A_i and B_i of both transfer functions and one obtains an overdefined system of non-linear equations which can be solved. These calculations were carried out

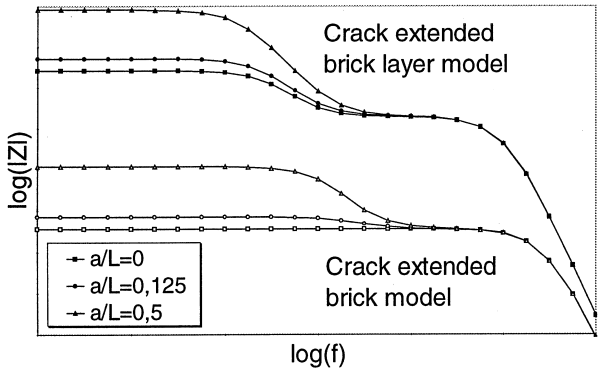

Fig. 5. Typical impedance spectra resulting from the crack extended models for different crack length and a definite opening of 2 μm.

using the software Maple.[13] The following relationships are established as the solution for the normalized quantities of the R-C elements and designated with the indices LF and HF:

$$r_{HF} = r_{gi}, c_{HF} = c_{gi}, \; r_{LF} = \frac{a_x}{L_x - a_x} r_{gi},$$
$$c_{LF} = \left(\frac{L_x}{a_x} - 1\right) c_{gi} + \frac{L_x}{a_x}\frac{L_y}{d_{gi}} c_A. \tag{9}$$

The equivalent circuit of the crack extended brick model according to Eq. (7) is mathematically equivalent to a network consisting of two R-C elements in series and therefore can be simplified in this way. The influence of the grains is exclusively determined by the quantities r_{HF} and c_{HF}. r_{LF} and c_{LF} are effective quantities which reveal the influence of the crack. Depending on the residual remaining cross-section $L_x - a_x$ the quantity r_{LF} gives that part of dc total resistance in the low-frequency ohmic range which is added after cracking. Therefore r_{LF} is a function of the crack length. The capacitance c_{LF} is not only determined by the crack length but also by the crack opening δ_y. The influence of the crack opening becomes clear if one inserts $c_A = \varepsilon_0 d_{gi}/\delta_y$ into the relationship for c_{LF} in Eq. (9). Therefore, the air volume of the crack determines c_{LF}.

Introducing the relationships of Eq. (4) the corresponding time constants $\tau_{HF} = r_{HF} c_{HF}$ and $\tau_{LF} = r_{LF} c_{LF}$ are given by

$$\tau_{HF} = \frac{\varepsilon_0 \varepsilon_{gi}}{\sigma_{gi}},$$
$$\tau_{LF} = \left(\varepsilon_{gi} + \frac{L_x}{L_x - a_x}\frac{L_y}{\delta_y}\right)\frac{\varepsilon_0}{\sigma_{gi}}. \tag{10}$$

The expression in parentheses for τ_{LF} in Eq. (10) is dominated by the second term. Since $a_x > 0$ it always follows that $L_x/(L_x - a_x) > 1$ and furthermore in the case of realistic cracks with small openings $L_y/\delta_y >> 1$ and in most cases $L_y/\delta_y >> \varepsilon_{gi}$ so that τ_{LF} is at least one order of magnitude higher than τ_{HF}. The crack damage results in two time constants which typically differ by more than one order of magnitude. Therefore, they both clearly appear in the spectra. Since τ is reversely proportional to ω one always recognizes the added time constant in the low-frequency range.

4.5. Simplified crack extended brick layer model

Considering the impedance spectra calculated by means of the crack extended brick layer model it seems reasonable to use also a network consisting of two R-C elements as a simplified model for a flawed two-phase microstructure. However, the difficulty lies in the fact that three phases have to be considered which are the grains, the grain boundary phases and the air-filled crack.

4.5.1. Approach by means of a network consisting of four R-C elements

In a mathematical respect, results from a series connection of four R-C elements a transfer function are given by.[12]

$$Z_S = \frac{\sum_{i=0}^{7} A_i \omega^i}{\sum_{i=0}^{4} B_{2i} \omega^{2i}}. \tag{11}$$

Eq. (6) can also be transformed to a rational function which is equivalent to Eq. (11). Comparing the coefficients of both forms one obtains a system of non-linear equations. Although this has no solution, an analytical approximation can be given by transmitting the results from Eq. (9) as follows[12]

$$r_1 = r_{gi}, \; c_1 = c_{gi}, \; r_2 = \frac{a_x}{L_x - a_x} r_{gi},$$
$$c_2 = \left(\frac{L_x}{a_x} - 1\right) c_{gi} + \frac{L_x}{a_x}\frac{L_y}{d_{gi}} c_A,$$
$$r_3 = r_{gb}, \; c_3 = c_{gb}, \; r_4 = \frac{a_x}{L_x - a_x} r_{gb}, \tag{12}$$
$$c_4 = \left(\frac{L_x}{a_x} - 1\right) c_{gb} + \frac{L_x}{a_x}\frac{L_y}{d_{gi}} c_A.$$

Making use of a network consisting of four R-C elements and the relationships in Eq. (12), one obtains a good agreement with the characteristic resulting from Eq. (6), as shown in Fig. 6. Deviations up to 1.1% merely occur in the frequency range from 100 to 1000 Hz.

Although only two time constants appear in the spectra, four time constants obviously describe the electrical behaviour. Taking Eq. (4) into account they are given by

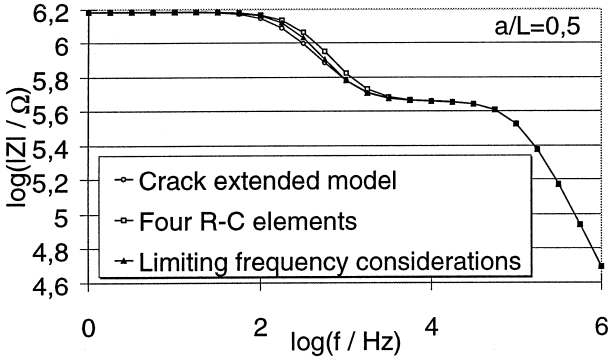

Fig. 6. Comparison of impedance spectra resulting from both simplified crack extended brick layer models and from the model according to Eq. (6) for different crack length and a definite opening of 2 μm.

$$\tau_1 = \frac{\varepsilon_0 \varepsilon_{gi}}{\sigma_{gi}}, \quad \tau_2 = \left(\varepsilon_{gi} + \frac{L_x}{L_x - a_x}\frac{L_y}{\delta_y}\right)\frac{\varepsilon_0}{\sigma_{gi}},$$
$$\tau_3 = \frac{\varepsilon_0 \varepsilon_{gb}}{\sigma_{gb}}, \tag{13}$$
$$\tau_4 = \left(\varepsilon_{gb} + \frac{d_{gb}}{d_{gi}}\frac{L_x}{L_x - a_x}\frac{L_y}{\delta_y}\right)\frac{\varepsilon_0}{\sigma_{gb}}.$$

It now strongly depends on the values of the time constants whether they appear clearly in the spectra or not. If two time constants almost have the same value the corresponding ohmic and capacitive ranges in each case are hardly to distinguish. They merge into one time constant.

The comparison of the time constants τ_2, τ_3 and τ_4 from Eq. (13) shows that these often hardly differ from each other. Since for the most polycrystalline ceramics the volume fraction of the grain boundary phase compared to the sample volume is always very small with $d_{gb}/d_{gl} << 1$ and further for short crack lengths it is $L_x/(L_x - a_x) < 2$, mostly in the expression for τ_4 follows although $L_y/\delta_y > > 1$ that $\varepsilon_{gb} > d_{gb}/d_{gi} \cdot L_x/(L_x - a_x) \cdot L_y/\delta_y$ or even $\varepsilon_{gb} > > d_{gb}/d_{gi} \cdot L_x/(L_x - a_x) \cdot L_y/\delta_y$ and therefore $\tau_4 \approx \tau_3$. If one considers the expression in parentheses for τ_2 it turns out that the second term is dominating because of $L_y/\delta_y >> 1$. With the assumed ratio for the conductivities $v_\sigma = \sigma_{gb}/\sigma_{gi} << 1$ one obtains for the time constant $\tau_2 \approx L_x/(L_x - a_x) \cdot v_\sigma \cdot \varepsilon_0/\sigma_{gb}$ which is mostly of the same scale as τ_3.

Hence, three time constants merge into one and the quantities of the corresponding R-C elements can be integrated as follows

$$r_{LF} = r_2 + r_3 + r_4, \frac{1}{c_{LF}} = \frac{1}{c_2} + \frac{1}{c_3} + \frac{1}{c_4}. \tag{14}$$

With the unchanged quantities r_1 and c_1 the final result is a network consisting of two R-C elements defined by the relationships in Eq. (15).

$$r_{HF} = r_1 = r_{gi}, \quad c_{HF} = c_1 = c_{gi},$$
$$r_{LF} = \frac{a_x}{L_x - a_x} r_{gi} + \frac{L_x}{L_x - a_x} r_{gb},$$
$$c_{LF} = \frac{\left(c_{gi} + \frac{L_x}{L_x - a_x}\frac{L_y}{d_{gi}} c_A\right)\left(c_{gb} + \frac{L_x}{L_x - a_x}\frac{L_y}{d_{gi}} c_A\right) c_{gb}}{\frac{L_x}{L_x - a_x} c_{gi}\left(c_{gb} + \frac{L_y}{d_{gi}} c_A\right) + \frac{L_x}{(L_x - a_x)^2}\frac{L_y}{d_{gi}} c_A \left((L_x + a_x) c_{gb} + L_x \frac{L_y}{d_{gi}} c_A\right) + \frac{a_x}{L_x - a_x} c_{gb}^2} \tag{15}$$

The quantity r_{LF} depends on the crack length and c_{LF} apart from that on the crack opening as in the case of the simplified crack extended brick model. Moreover, one obtains characteristics which can not be distinguished from the comparable characteristics of the corresponding network consisting of four R-C elements. The general description of the electrical behaviour with a network consisting of four R-C elements is only required in exceptions because under the given conditions as well as in the case of realistic polycrystalline two-phase microstructures and crack damages for the time constants is mostly valid: $\tau_2 \approx \tau_3 \approx \tau_4$. Therefore, the crack extended brick layer model can be typically simplified as a network consisting of two R-C elements in series.

4.5.2. Approach by means of limiting frequency considerations

The influence of the crack is only effective on the low-frequency range of the impedance spectra as shown in Fig. 5. In particular with increasing crack length the magnitude of the low-frequency ohmic range clearly increases. In the high-frequency ohmic and the high-frequency capacitive range obviously no changes occur. Consequently, the quantities r_{gi} and c_{gi} which describe the electrical behaviour of the grains remain unchanged.[12] If therefore one employs a network consisting of two R-C elements for modelling the other two quantities can be determined from limiting frequency considerations. Eq. (6) can be simplified for $\omega << 1/\tau_{gb}$ as follows

$$Z_{S,LF} = \frac{M_y}{N_x K_z}\left(R_{gi} + R_{gb}\right)\frac{L_x}{L_x - a_x} = R_{res}. \tag{16}$$

An ohmic current flow exclusively occurs through the grains and across the grain boundary phases in the remaining flawless cross section. In the equivalent circuit, this corresponds to a series connection of two ohmic resistors where the normalized resistance occurring in the high-frequency range is known and amounts:

$$r_{HF} = r_{gi}. \tag{17}$$

Consequently the second resistance may be determined by the difference of $N_x K_z d_{gi}/M_y \cdot R_{res} - r_{HF}$ as:

$$r_{LF} = \frac{a_x}{L_x - a_x} r_{gi} + \frac{L_x}{L_x - a_x} r_{gb}. \tag{18}$$

For high frequencies with $\omega >> 1/\tau_{gi}$ one obtains from Eq. (6) for the sample impedance Eq. (19).

$$Z_{S,HF} = -j\frac{1}{\omega}\frac{M_y}{N_x K_z}\left(\frac{1}{C_{gi}} + \frac{1}{C_{gb}}\right) \frac{\frac{L_y}{d_{gi}}\left(\frac{1}{C_{gi}} + \frac{1}{C_{gb}}\right) + \frac{1}{c_A}}{\frac{L_y}{d_{gi}}\left(\frac{1}{C_{gi}} + \frac{1}{C_{gb}}\right) + \left(1 - \frac{a_x}{L_x}\right)\frac{1}{c_A}} = -j\frac{1}{\omega}\frac{1}{C_{res}} \tag{19}$$

Now the current flows through the grains, across the grain boundary phases and over the air gap exclusively as a displacement current. In the equivalent circuit this has to be identified with a series connection of two capacitors where the very much smaller capacitance of the volume fraction of the grains still dominates the electrical behaviour in the high-frequency range. This remains unchanged due to a crack and amounts in the normalized form:

$$c_{HF} = c_{gi}. \tag{20}$$

By solving and normalizing the relationship $1/C_{res} = 1/C_{HF} + 1/C_{LF}$ one obtains with $c_A = C_A/d_{gi}$ the second capacitance as:

$$c_{LF} = \frac{\left(1 - \frac{a_x}{L_x}\right)c_{gi}c_{gb} + \frac{L_y}{d_{gi}}(c_{gi} + c_{gb})c_A}{\frac{a_x}{L_x}c_{gb} + c_{gi} + \frac{L_y}{d_{gi}}(c_{gi} + c_{gb})\frac{c_A}{c_{gb}}}. \tag{21}$$

Fig. 6 shows the characteristics according to both approximations and the one following from Eq. (6).

The approach using the limiting frequency considerations achieves a very high agreement with the former model and therefore can describe the typical electrical behaviour of a flawed two-phase microstructure. Deviations only up to 0.6% occur.

4.5.3. Comparison of both approaches

Comparing the two simplified models one recognizes that the expressions for r_{LF} according to Eqs. (15) and (18) are identical. Differences exist between the analytical expressions for the capacitances c_{LF} according to Eqs. (15) and (21) which however lead to very similar numerical results. The simplification of the crack extended brick layer model to a network consisting of two R-C elements performs with the approach by means of the limiting frequency considerations a higher agreement with the former, crack extended model than with the approach using a network consisting of four R-C elements. Nevertheless the approach according to Eqs. (18) and (21) represents the general case. In special cases this the only one which can be used for a simplification as shown later.

4.6. Numerical field computations

Numerical computations of the electrical fields were used in order to consider the deviations resulting from the assumption of one-dimensional current flow and to correct the simplified crack extended models.

The calculations were carried out with the software MAFIA and Maxwell[14,15] using the geometrical data as in the respective experiments. However, for reasons of a limited computer performance the geometries were reduced to the two-dimensional case. For each simulated field always a surrounding atmosphere in addition to the sample with the electrical properties $\varepsilon_A = 1$ and $\sigma_A = 0$ as well as open limiting conditions were used. The electrodes were considered as ideal electrical conductors. For the electrical properties of the individual phases, specific values must be taken. Since the calculations are very extensive, a general processing with parameter variations of the sample geometry or of the electrical properties within the framework of the present work is not possible. Therefore, the electrical properties for the flawless materials determined from the experiments and by means of the brick layer model are employed for these calculations. The crack was modelled as an air-filled rectangle with a definite opening $\delta_y = 2$ μm and the electrical properties $\varepsilon_A = 1$ and $\sigma_A = 0$. All computations were carried out for cracks of variable length running parallel to the electrodes.

4.6.1. Quasi static field

If one excites the sample at elevated temperatures with an ac voltage, the complex current consists of a dielectric displacement part and an ohmic part. From the viewpoint of the electrical field theory for the description of the electrical behaviour a quasi static field may be applied, because the wavelength $\lambda = c_0/f$ and the skin depth of the electrical field $\delta = 2^{1/2}(\sigma\mu_0\omega)^{-1/2}$ with values of 300 and 50 m at the upper limiting frequency of $f = 1$ MHz and in the case of a conductivity of $\sigma = 10^{-4}$ S/m are a lot higher than the geometrical measurements of the sample which are in the mm-range. One obtains the complex current as a secondary quantity for every calculation at a specific frequency and can compute the impedance $Z = U/I$ using the given voltage.

In order to determine numerically an impedance spectrum many footholds are required in the frequency band. The number and location of the footholds was chosen as in the experiments with four frequency points per decade. Therefore, 25 field calculations in total are required for a spectrum from 1 Hz to 1 MHz.

4.6.1.1. 9Ce-TZP. The sample can not be regarded as an homogeneous material. On the contrary the microstructure consisting of grains and grain boundary phases with their specific electrical properties must be considered. For the electrical properties of both phases of 9Ce-TZP the data specific at 400°C obtained by means of the brick layer model were employed: $\varepsilon_{gi} = 38$, $\sigma_{gi} = 1.9\times10^{-4}$ S/m, $\varepsilon_{gb} = 19$ and $\sigma_{gb} = 3.4\times10^{-7}$ S/m. It would be desirable to idealize the microstructure according the brick layer model as an array of cubic grains of a size that corresponds to the real, mean grain size of 1.2 μm and with covering grain boundary films of a thickness of 1.4 nm. However, one rapidly runs into the limits of the performance from computers. Therefore,

the microstructure must be reproduced more coarsely with clearly bigger and less grains than in reality.

It turned out that a suitable compromise represents a microstructure, as shown in Fig. 7, which contains 233 grains of different size in total.[12]

Structuring was coarsely chosen in flawless regions and was increasingly refined to the damaged area since there the conductivity occurs not only normal to the electrodes and therefore an influence of the structuring on the result may be expected. The sum from the grain size and from the proportional grain boundary film thickness amounts 2 mm in the biggest and 0.125 mm in the finest case. The refinement was carried out in each case by bisectioning of the measurements. In the region of the finest structuring the thickness of a grain boundary phase is 0.15 μm. Even the thickness of the biggest grain boundaries is so small that it is not recognizable in Fig. 7. The crack is in the middle of the sample as in the comparable experiment, has its beginning at the bottom and runs parallel to the electrodes. A purely intergranular cracking is always considered which means that the crack runs along the grain boundaries and divides no grains.

Complete spectra were then computed for two different crack lengths. Qualitatively, one finds the same facts as in the case of the spectra which were calculated by means of the crack extended brick layer model. Changes also occur in the low-frequency range. In particular, an increasing magnitude of the low-frequency ohmic range appears again with increasing crack length in the spectra. The result is represented in Fig. 17 compared with the characteristics of the corrected, crack extended brick layer model which is subject to Section 5.2.

4.6.1.2. 8YSZ. Only one phase has an effect from the electrical respect in the case of 8YSZ. Therefore, the microstructure can be idealized as a continuous phase.

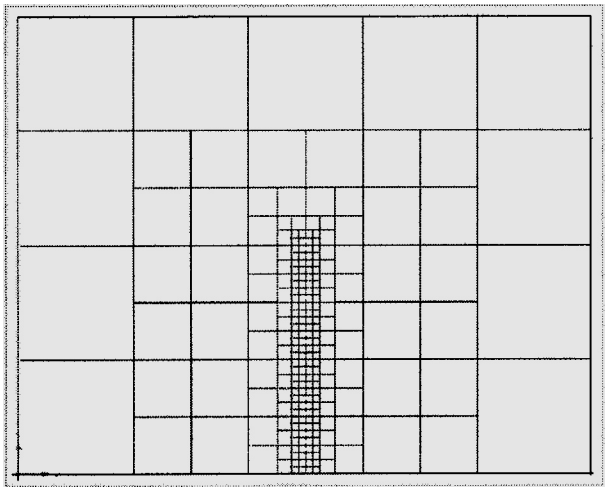

Fig. 7. Idealized graded microstructure for the numerical field computations.

The following electrical properties were employed for the field calculations: $\varepsilon_{gi} = 30.6$, $\sigma_{gi} = 7.76 \times 10^{-4}$ S/m. The crack is again in the middle of the sample and runs parallel to the electrodes. Complete spectra were then computed for different crack lengths as shown in Fig. 8.

As predicted with the crack extended brick model a second electrical time constant in the low-frequency range results from a crack damage in the spectra obtained by the numerical field computations. Again, one finds an increasing magnitude of the low-frequency ohmic range with increasing crack length which becomes especially clear in the case of the spectrum for a crack of the related length $a_x/L_x = 0.5$.

4.6.2. Electrostatic field

In the case of high frequencies where the material behaves purely capacitive the electrostatic field can be applied. Then, the sample can be regarded as an ideal, homogeneous, dielectric of the effective permittivity $\varepsilon = 38$ for 9Ce-TZP. For each crack length the electrical field and as a secondary quantity the stored charge of the system was computed. Consequently, the total capacitance and the effective permittivity of the arrangement can be determined. These results are compared with the

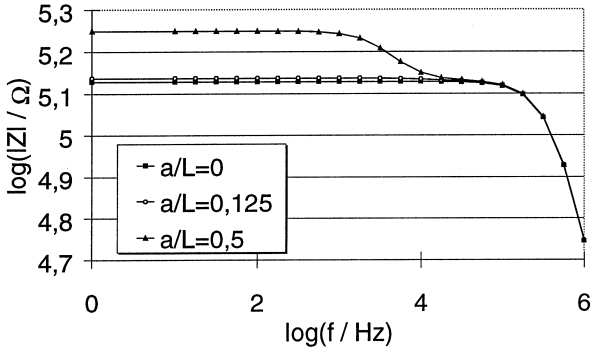

Fig. 8. Numerically from the quasi static fields computed Bode characteristics for a 8YSZ sample with different crack lengths.

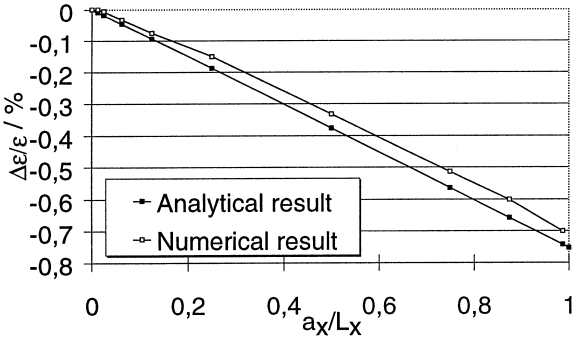

Fig. 9. Numerically from the electrostatic field and analytically with the crack extended brick layer model for high frequencies computed relative decreases of the effective permittivity depending on the related crack length in the case of a crack opening $\delta_y = 2$ μm.

analytical calculations according to Eq. (19) as relative changes, as shown in Fig. 9.

One observes a linear decrease in the curve resulting from the analytical calculations which amounts for a completely cracked sample −0.75% ($a_x/L_x = 1$). From the numerical field computations always follows a smaller relative decrease of the permittivity. The ratio of both values enters as a correction factor for the extended model as shown later.

Fig. 9. Numerically from the electrostatic field and analytically with the crack extended brick layer model for high frequencies computed relative decreases of the effective permittivity depending on the related crack length in the case of a crack opening $\delta_y = 2$ μm.

4.6.3. Direct current flow field

These calculations were carried out for the verification of the low frequency behaviour of the crack extended brick layer model and also enter in its correction. Since the conductivity of the grains and of the grain boundary phases differ clearly unlike the permittivity, the microstructure must be considered here. This is implemented using the microstructure shown in Fig. 7. The resulting electric flux course of the simulated dc behaviour of a flawed 9Ce-TZP sample with the assumption of a grain conductivity $\sigma_{gi} = 1.9 \times 10^{-4}$ S/m and a conductivity in the grain boundary phases $\sigma_{gb} = 3.4 \times 10^{-7}$ S/m is shown in Fig. 10.

It is quite obvious that one-dimensional current flow only occurs in flawless regions far away from the crack. Therefore the effective conductivity for flawed material is higher than that one obtains from the crack extended model under the assumption of one-dimensional current flow over the remaining flawless cross section. This was expected. The question now is how big the quantitative differences are.

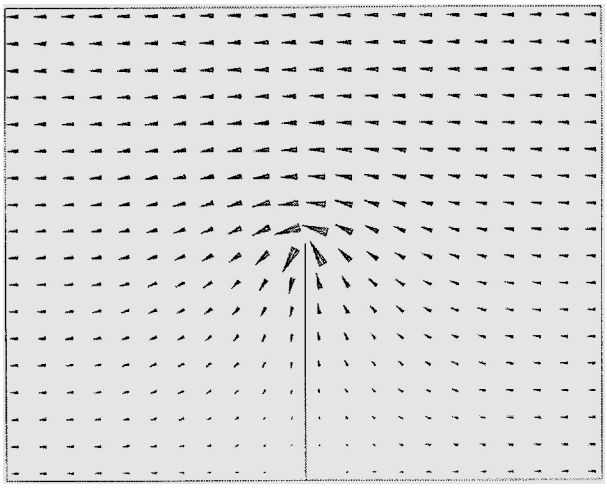

Fig. 10. Electrical field at dc current flow in the sample with a crack of $a_x = 4$ mm ($a_x/L_x = 0.5$) length and an opening of $\delta_y = 2$ μm.

Numerical computations of the dc current were carried out for different crack lengths and a definite crack opening of $\delta_y = 2$ μm and then compared in each case with the results from the crack extended brick layer model for low frequencies according to Eq. (16).

Depending on the related crack length both characteristics for the relative decrease of the effective total conductivity are shown in Fig. 11.

A linear decrease which is proportional to the related crack length results from the analytical solution. For a completely cracked sample the decrease amounts −100%, which means of course, that no dc current flow is possible. From the numerical computations on the other hand, one notices a by far smaller relative decrease of the total conductivity, in particular for medium-sized crack lengths. For example amounts the relative decrease for a sample with a crack of the related length $a_x/L_x = 0.5$ only the half of the value resulting from the analytical calculation.

4.7. Comparison of the results from the model and the numerical field computations

Qualitatively, the spectra resulting from the numerical computations of the quasi static electrical field are very similar as the spectra determined with the crack extended brick layer model. However, there are differences in the low-frequency range in quantitative respect. By means of the numerical computations of the static fields which are less time consuming than the computations of the quasi static fields the corresponding quantities in the simplified equivalent circuit for the crack extended brick layer model consisting of two R-C elements in series can now be corrected. For the quantity r_{LF} the computations of the dc current field have to be considered. From these calculations one obtains the true total conductivity or the true total resistance r_{total} of the sample. According to the model at low frequencies [see Eq. (16)] the total resistance is given by $r_{res} = r_{LF} + r_{HF}$. From the ratio of these two resistances a correction factor $k_r = r_{total}/r_{res}$

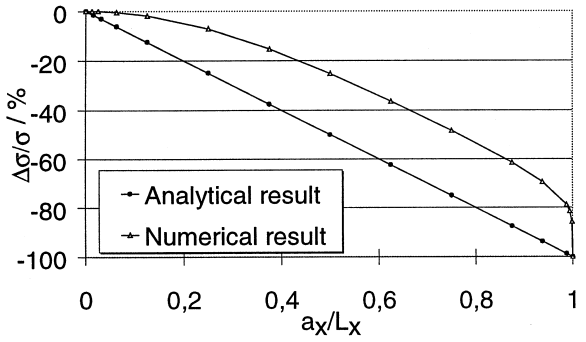

Fig. 11. Numerically from the dc current flow field and analytically with the crack extended brick layer model for low frequencies computed relative decreases of the effective conductivity depending on the related crack length.

depending on the crack length can be derived. Since r_{HF} is known from the impedance measurements and remains unchanged due to a crack damage the other ohmic resistance in the simplified crack extended brick layer model can be corrected and its true value is given by

$$r_{LF,corr} = k_r(r_{HF} + r_{LF}) - r_{HF}. \quad (22)$$

With the analytical model calculations one overestimates r_{res} and thus r_{LF}. Therefore, r_{LF} must be corrected downwards and it applies: $0 < k_r \leqslant 1$. The larger the crack length is, the stronger the correction has to be and the smaller becomes k_r. At the same time r_{LF} strongly increases and therefore it always applies: $r_{LF,corr} > 0$. Since the crack opening is small compared to the thickness of the sample with $\delta_y << L_y$, k_r does not depend on δ_y. However, the thickness of the sample has an effect on k_r if this is not much larger than the crack length. A larger sample thickness means here a smaller volume density of cracks. Therefore the contribution of r_{LF} is smaller and a stronger correction is necessary, which becomes effective in a smaller k_r, as shown in Fig. 12, for two different thicknesses of the sample.

The quantity c_{LF} can be corrected analogously. Here, the computations of the electrostatic field have to be considered and the true total capacitance of the sample c_{total} is employed. Via the relationship $c_{res}^{-1} = c_{LF}^{-1} + c_{HF}^{-1}$ which follows from simplified crack extended brick layer model at high frequencies according to Eq. (19), the corrected value of the capacitance appearing in the low-frequency range is given by

$$c_{LF,corr} = \frac{k_c c_{HF}}{\frac{c_{HF}}{c_{LF}} + 1 - k_c} \quad (23)$$

if one introduces the correction factor $k_c = c_{total}/c_{res}$. Since it is now only a question of a displacement current which can also flow across the crack, the deviations of the model computations are considerably smaller than before. Therefore, only small corrections are necessary and the values of k_c are close to one. Apart from the crack length this correction factor always depends on the crack opening as well as on the sample thickness. Fig. 13 shows the characteristics of k_c as a function of the related crack length for different values of δ_y as well as for different sample thicknesses.

If one employs the corrected quantities $r_{LF,corr}$ and $c_{LF,corr}$ ($k_r = 0.68$ and $k_c = 1.00068$) as well as the unchanged quantities r_{HF} and c_{HF} the impedance spectra resulting from the corrected, crack extended brick layer model with an equivalent circuit consisting of two R-C elements in series correspond very well with the spectra obtained by means of the numerical computations of the quasi static field, as shown in Fig. 14, for a sample with a crack of a length of $a_x = 4$ mm. Merely in the capacitive transition region small deviations can be found which however became less by the correction. In the low-frequency ohmic range there is even a complete agreement of both characteristics after the correction. For comparison, the corresponding characteristic of the former, crack extended brick layer model is also represented in Fig. 14.

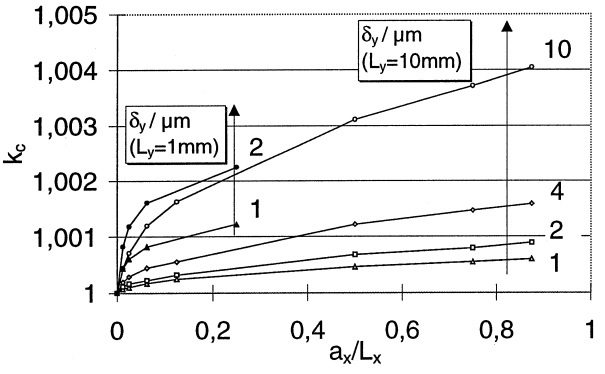

Fig. 13. Correction factor k_c for the simplified crack extended brick layer model resulting from the numerical computations of the electrostatic fields depending on the related crack length.

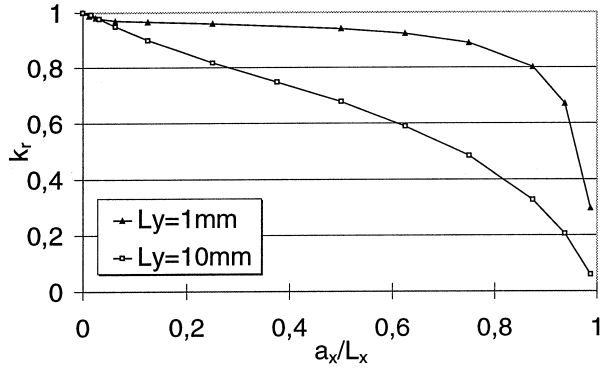

Fig. 12. Correction factor k_r for the simplified crack extended brick layer model resulting from the numerical computations of the static field in the case of dc current flow versus the related crack length.

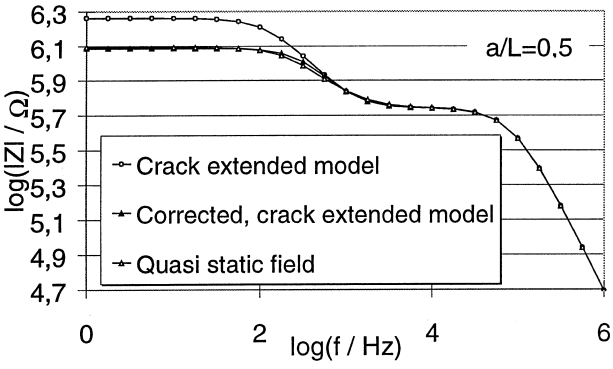

Fig. 14. Comparison of the Bode characteristics resulting from the numerical computations of the quasi static fields and from the corrected crack extended brick layer model.

5. Discussion

5.1. Microstructure of the flawless zirconia ceramics and modelling

A continuous grain boundary phase could be proved by TEM investigations including EDX analyses in the TZP materials. These results imply the use of the brick layer approach for modelling. In contrast to this in 8YSZ such a distinctive second phase was not found. A second phase in the triple points can definitely be excluded. No contribution or only a very small contribution to the grain boundary blocking effect in the impedance spectra was also found in previous investigations on comparable materials.[11,16] This points to a very high purity of the raw material as well as a very low porosity of the specimens used here and therefore, modelling the 8YSZ with the brick model is justified. For all investigated materials the interface electrode/ceramic does not appear in the impedance spectra.[12]

5.2. Modelling of flawed zirconia ceramics inclusive the numerical field computations and comparison with the experimental results

Employing the electrical properties of the phases obtained from the experimental data for 9Ce-TZP at 400°C and by means of the brick layer model: $\varepsilon_{gi} = 38$, $\sigma_{gi} = 1.9 \times 10^{-4}$ S/m, $\varepsilon_{gb} = 19$ and $\sigma_{gb} = 3.4 \times 10^{-7}$ S/m as well as crack data with an opening of $\delta_y = 2$ μm and different crack lengths one obtains from the simulation with the crack extended brick layer model [according to Eq. (6)] characteristics which are qualitatively very similar with the characteristics resulting from the experiments (see Figs. 2 and 5). Therefore, with the crack extended brick layer model the electrical behaviour of a flawed sample can qualitatively be described. Furthermore, this model could be simplified in the form of a network consisting of two R-C elements in series by means of limiting frequency considerations or by transferring to a network consisting of four R-C elements in series and physically understandable correlations with the microstructure as well as the crack can be set up. With both simplified approaches, one obtains the same total resistance in the low-frequency range and therefore the quantity r_{LF} according to Eq. (15) and (18). r_{LF} is an effective quantity that is determined both by the resistances of the grains and of the grain boundary phases and by the crack length. The determination of the capacitance in the low-frequency range is not unambiguous with the simplified models since it is not a question of a purely capacitive range. However, the predominantly capacitive transition region can well be approximated with a capacitance which is designated in standardized form with c_{LF}. This quantity can be given in analytical forms according to Eqs. (15) and (21). It depends besides on the capacitances of the volume fraction of the grains and of the volume fraction of the grain boundary phases also on the crack length and on the crack opening. The simplification of the crack extended brick layer model to a network consisting of two R-C elements performs with the approach by means of the limiting frequency considerations a higher agreement with the former crack extended model and will be used in the following.

In the case of a single-phase microstructure, the simplified crack extended brick model together with the quantities from the relationships in Eq. (9) is qualitatively able to reproduce the electrical behaviour of a 8YSZ sample with an individual crack as it was found in the experiment (see Fig. 3). For the calculations of the spectra the electrical data: $\varepsilon_{gi} = 30$, $\sigma_{gi} = 7.8 \times 10^{-4}$ S/m and cracks of variable lengths and an opening of $\delta_y = 2$ μm were considered (see Fig. 5).

Finally, by means of the numerical computations of the corresponding electrical fields it was possible to correct the deviations in the simplified crack extended models resulting from the assumption of one-dimensional current flow. The correction factors for the quantities r_{LF} and c_{LF} can be determined from the static, electrical fields for dc current flow and pure displacement current. Compared to the numerical computations of the quasi static field, which were also computed for control purposes, these calculations are a lot less time-consuming.

Hence the simulation of the spectra of flawed 2Y- and 9Ce-TZP samples is based on the corrected, simplified, crack extended brick layer model and the simulation of the 8YSZ materials on the corrected, simplified, crack extended brick model. In both cases, the quantities appearing in the low-frequency range of the spectra are decisive with regard to the qualitative and quantitative influence of the crack damage.

5.2.1. Flawed 9Ce-TZP

In several experiments on 9Ce-TZP samples, a multiple prolongation of a short starting crack could be achieved. The characteristics for the relative decrease of the conductivity and the relative decrease of the capacitance of the optimized quantities r_{LF} and c_{LF} represented in Fig. 15 result from the experiment shown in Fig. 2.

These refer to the initial state in each case and depend on the related crack length. Both characteristics are typically for all experiments carried out. They decrease approximately linearly to the related crack length, the relative decrease of the capacitance is a little stronger.

If one employs the quantities $r_{LF,corr}$ and $c_{LF,corr}$ of the corrected, crack extended brick layer model according to Eqs. (22) and (23), a quantitative comparison with the relative decreases experimentally determined can be drawn. Considering Eq. (18) and the relationships in Eq. (4) one obtains the relative decrease of the conductivity from the model calculations given by Eq. (24).

$$\frac{\Delta\sigma_{\mathrm{LF,corr}}}{\sigma_{\mathrm{LF,corr}}} = -\frac{\sigma_{\mathrm{gb}} + \dfrac{d_{\mathrm{gb}}}{d_{\mathrm{gi}}}\sigma_{\mathrm{gi}} - k_{\mathrm{r}}\dfrac{L_x}{L_x - a_x}\left(\sigma_{\mathrm{gb}} + \dfrac{d_{\mathrm{gb}}}{d_{\mathrm{gi}}}\sigma_{\mathrm{gi}}\right)}{\sigma_{\mathrm{gb}} - k_{\mathrm{r}}\dfrac{L_x}{L_x - a_x}\left(\sigma_{\mathrm{gb}} + \dfrac{d_{\mathrm{gb}}}{d_{\mathrm{gi}}}\sigma_{\mathrm{gi}}\right)} \tag{24}$$

As long as the crack opening and the crack length are small compared to the thickness of the sample as $\delta_y << L_y$ and $a_x < L_y$ the correction factor k_{r} only depends on the crack length, but not on the crack opening. The relative decrease of the conductivity also only depends on a_x. If one draws the relative decrease of the conductivity determined according to Eq. (24) versus the related crack length, where the specific electrical properties of the phases at 400°C and k_{r} from Fig. 12 were employed one also lists an almost linear function, as shown in Fig. 16.

Therefore, with respect to the conductivity, the model calculations quite well represent the characteristics found experimentally in Fig. 15.

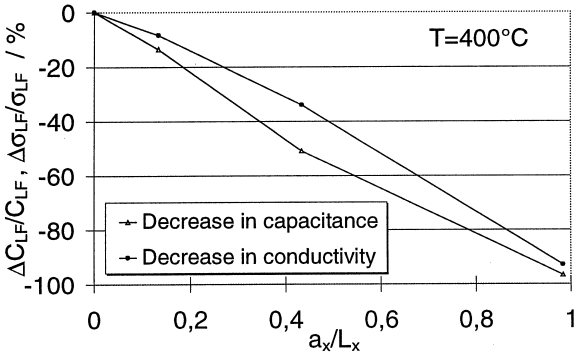

Fig. 15. Relative decreases of the capacitance and of the conductivity for the low-frequency quantities calculated from measured spectra at 400°C due to a crack depending on the related crack length.

The decrease of the capacitance depends on the crack length and also on the crack opening according to Eq. (23). If one takes Eq. (4) into account the relative decrease of the capacitance is given by Eq. (25).

Fig. 16 also shows the characteristics of the relative decreases of the capacitance for different crack openings where the corresponding correction factors have been used. For a definite crack opening the relative decrease is stronger than linear and especially high for short crack lengths. Given that the crack opening always becomes larger with increasing crack length and considering both, the relative decreases experimentally determined as shown in Fig. 15 and computed according to Eq. (25), one estimates for the crack openings up to 1 μm for short cracks and 2 to 10 μm for long cracks. This is in realistic orders of magnitude and therefore the corrected, crack extended model can be used to realistically describe the changes of the electrical behaviour resulting from a crack damage with the quantities $r_{\mathrm{LF,corr}}$ and $c_{\mathrm{LF,corr}}$. The model calculations represent a good basis for estimates concerning the minimum size of a crack damage which is recognizable by impedance measurements as shown later.

For verifying both, the idealized microstructure according to Fig. 7 and the corrected, crack extended brick layer model numerical computations of the quasi static electrical field for a sample with an individual crack were employed. Fig. 17 shows the impedance spectra,

$$\frac{\Delta c_{\mathrm{LF,corr}}}{c_{\mathrm{LF,corr}}} = -\frac{\left[\left(1 - \dfrac{a_x}{L_x}\right)k_{\mathrm{c}} - 1\right]c_{\mathrm{gi}}c_{\mathrm{gb}} + \dfrac{L_y}{d_{\mathrm{gi}} + d_{\mathrm{gb}}}(k_{\mathrm{c}} + c_{\mathrm{gb}})c_{\mathrm{A}}}{\left[\left(1 - \dfrac{a_x}{L_{\mathrm{x}}}\right)k_{\mathrm{c}}\dfrac{c_{\mathrm{gb}}}{c_{\mathrm{gi}} + c_{\mathrm{gb}}} - 1\right]c_{\mathrm{gi}}c_{\mathrm{gb}} + \dfrac{L_y}{d_{\mathrm{gi}} + d_{\mathrm{gb}}}\left[(k_{\mathrm{c}} - 1)c_{\mathrm{gb}} - c_{\mathrm{gi}}\right]c_{\mathrm{A}}} \tag{25}$$

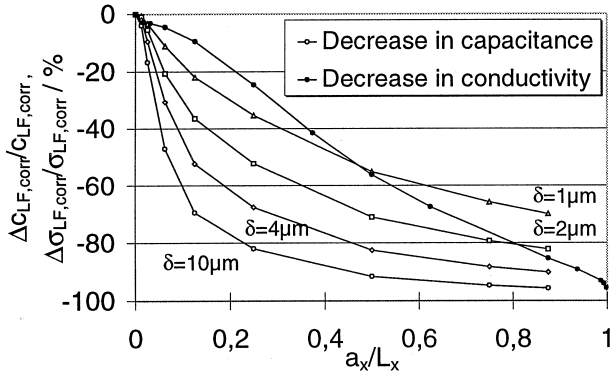

Fig. 16. Relative decreases of the capacitance and of the conductivity for the low-frequency quantities computed by means of the corrected, crack extended brick layer model depending on the related crack length.

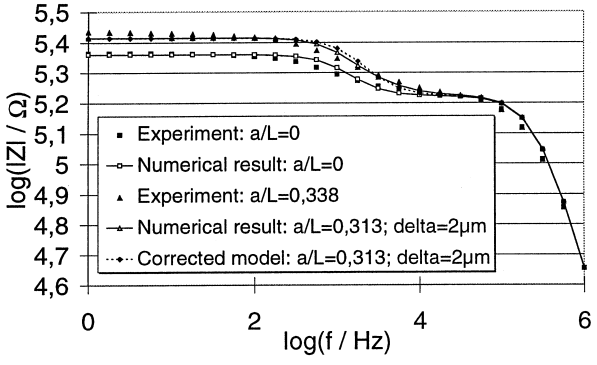

Fig. 17. Comparison of the impedance spectra determined as well experimentally as with the corrected, crack extended brick layer model as with the numerical computations of the quasi static field for a 9Ce-TZP sample with and without a crack.

both, for the initial state and for the flawed state determined as well experimentally as from the corrected, crack extended brick layer model as from the computations of the quasi static field.

A crack length of $a_x = 2.7$ mm ($a_x/L_x = 0.338$) was found in the experiment. For the calculations in each case a crack length of $a_x = 2.5$ mm ($a_x/L_x = 0.313$) and a crack opening $\delta_y = 2$ μm were used. Apart from small deviations in the capacitive ranges there is a good agreement between the measured characteristics and the characteristics resulting from the numerical computations of the quasi static fields as well as from the corrected, crack extended model for both, the flawless and the flawed state. As a result, the corrected, crack extended brick layer model is confirmed by the purely numerical computations as well as by the experiment.

5.2.2. Flawed yttria-stabilized zirconia

Qualitatively, the electrical behaviour of 2Y-TZP does not differ from that of 9Ce-TZP (see Fig. 3). In the case of 8YSZ, however, one finds an additional, second time constant in the low-frequency range of the spectra due to a crack (see Fig. 3). Therefore, the electrical behaviour of 8YSZ will be regarded in the following only. The two new quantities are designated with r_{LF} and c_{LF}.

In the experiment, the crack length was $a_x/L_x = 0.76$. The additional capacitance is around 550 times larger than the corresponding capacitance of the volume fraction of the grains. By means of the corrected, crack extended brick model the crack opening according to Eqs. (9) and (23) can be estimated to $\delta_y = 0.8$ μm. The additional resistance is as big as the resistance of the volume fraction of the grains resulting from the measured spectra. Employing the crack data in Eq. (9) and with the corresponding correction factor $k_r = 0.484$ follows from the corrected, crack extended model according Eq. (22) an additional resistance $r_{LF,corr} = 1.02 \cdot r_{gi}$. Hence, a very good agreement of the experiment and the model exists. Furthermore, the spectra resulting from the numerical computations of the quasi static field are in very good correspondence with those resulting from the corrected, crack extended brick model and consequently, confirm it as well.

5.3. Limits and possibilities of impedance measurements for damage detection in structural ceramics

5.3.1. Size of detectable damages in zirconia ceramics

For the following estimates 9Ce-TZP is considered. The electrical properties of the phases in the flawless, initial state at 400°C are employed.

By means of dc measurements at elevated temperatures, the ohmic total resistance of the sample is registered where the information content and the measuring sensitiveness are smaller than in the case of frequency-dependent ac measurements. Those reflect a differentiated electrical behaviour of the single phases in the impedance spectra. The estimates are based on the corrected, crack extended brick layer model using the numerical computations of the static electrical fields. One obtains the information about the influence of the crack damage from the quantities of the R-C element which determine the low-frequency range of the spectra.

Fig. 18 shows the relative decrease of the conductivity due to an individual crack depending on the crack length for a sample of a thickness of $L_y = 10$ mm, a width of $L_x = 8$ mm and a length of $L_z = 12$ mm computed from the quantity $r_{LF,corr}$. This sample geometry was determined by the conditions of the experiment. In the case of thinner samples but otherwise identical data the measuring sensitiveness increases for example from 1 to 8% for a crack of the length $a_x/L_x = 0.05$ in a sample of a thickness of $L_y = 1$ mm, as shown in Fig. 18.

The corresponding correction factor k_r can be found in Fig. 12. Independent from the sample thickness the relative changes in the quantities $r_{LF,corr}$ or $\sigma_{LF,corr}$ due to a crack are at least around a factor 4 for $a_x/L_x > 0.0125$ and up to two orders of magnitude in the case of long cracks higher than the relative changes in the effective permittivity at room temperature.[12]

The relative changes of $c_{LF,corr}$ with respect to the initial state calculated for samples of the same geometries as before are considerably higher than those of $\sigma_{LF,corr}$ as shown in Fig. 19.

For example, the relative change of $c_{LF,corr}$ in a sample which is 1 mm thick amounts to −43% for $a_x/L_x = 0.05$, $\delta_y = 1$ μm and to approximately −5% for $a_x = 100$ μm ($a_x/L_x = 0.0125$), $\delta_y = 1$ μm. The corresponding correction factors k_c were computed for both sample thicknesses (see Fig. 13). In addition here, the crack opening has clear effects on the result. The absolute value of the relative decrease of the capacitance increases with an increasing crack opening. For $a_x =$

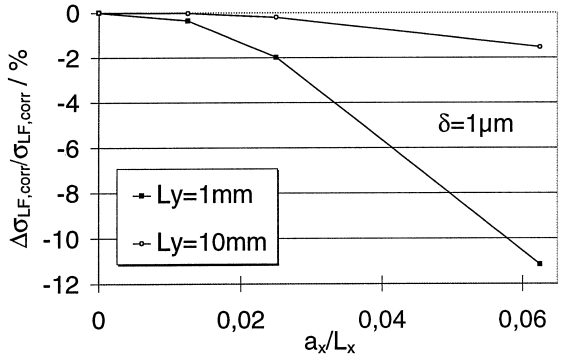

Fig. 18. Relative changes in conductivity depending on the related crack length a_x/L_x calculated with the corrected, crack extended brick layer model for two different sample thicknesses and a definite crack opening of $\delta_y = 1$ μm.

100 μm and $\delta_y = 2$ μm the relative decrease $\Delta c_{LF,corr}/c_{LF,coor}$ amounts to −8%.

In total, the quantity $c_{LF,corr}$ shows the highest sensitivity to a crack damage which can lead to measuring effects of far more than 10% in the case of short cracks with an opening of $\delta_y = 1$ μm. If the crack opening is by far less than 1 μm, the changes in electrical respect still have a significant effect in the quantity $\sigma_{LF,corr}$. The sample geometry as well as the electrode arrangement also have strong effects on the measuring sensitiveness.

5.4. Transfer of the results to other materials

The brick layer model is a good description for flawless two-phase microstructures when the grains show a by far higher conductivity than the grain boundaries and the grains are completely covered by the grain boundary phase. If in such a material a crack damage occurs the corrected, crack extended brick layer model can be always applied. Hence, the effects on the electrical behaviour due to a crack of a great number of materials can be predicted in qualitative and quantitative respect. In the case of single-phase microstructures the brick model in the initial state and the corresponding crack extended model in the flawed state is suitable.

In order to find an ideal material for the detection of a crack in it by means of impedance measurements with a maximum measuring sensitivity, one varies the electrical properties and the ratio of the thicknesses of both phases and employs the corrected, crack extended brick layer model. This material is characterized by the following properties of the grain boundary phase:[12] its conductivity is likely as close as possible at the upper boundary value with $\sigma_{gb} \leqslant 0.1\sigma_{gi}$, its effective permittivity is as high as possible in relation to this of the grains and its thickness is as small as possible.

5.5. Effects of a crack damage on the number of distinguishable electrical time constants in the impedance spectra

Comparing the rational transfer function of the brick layer model for the flawless state which corresponds mathematically to the form of Eq. (8) with that of the crack extended brick layer model according Eq. (11), one notices that its order is doubled due to a crack. Analogously, a doubling occurs from two to four in the case of the brick model and the crack extended version. This means that the number of time constants is doubled by a crack damage, as shown in principle in Fig. 20.

However, the impedance spectra of realistic, flawed polycrystalline materials are typically characterized by two time constants, as shown before. At least in theoretical respect, there exist special cases where three time constants clearly appear over a frequency range from 1 Hz to 1 MHz. This can be expected particularly if the volume fraction of the grain boundary phase is no longer small compared to the volume of the sample. In the relationships of Eq. (13) follows that $\tau_4 >> \tau_3$ and consequently at very low frequencies a third time constant appears in the spectrum, as shown by the following example. If the volume fraction of the grain boundary phase of a material amounts $x_{gb} = 0.15$ and the following electrical properties: $\varepsilon_{gi} = 38$, $\sigma_{gi} = 10^{-4}$ S/m, $\varepsilon_{gb} = 19$ and $\sigma_{gb} = 10^{-6}$ S/m are employed one obtains using the brick layer model for a sample of the size $10 \times 8 \times 12$ mm^3 in the initial state and using the crack extended brick layer model for this sample with a crack of a length of $a_x = 4$ mm ($a_x/L_x = 0.5$) and an opening of $\delta_y = 2$ μm the Bode characteristics as shown in Fig. 21.

This fictitious material would have similar electrical properties as 9Ce-TZP at 400°C, however, the volume fraction of the grain boundary phase is considerably larger as in reality. In the spectrum for this material with a crack one really lists another qualitative behaviour as in the flawless state. At low frequencies, the expected third time constant can be clearly observed. A simplification of the crack extended brick layer model according to Eq. (6) is only possible using the approach with the network consisting of four R-C elements. In the final analysis one obtains a series connection of three R-C elements which describes the electrical behaviour.

For control purposes the numerical computations of the corresponding quasi static field are now considered. The characteristic obtained numerically is very similar. Three time constants as in the case of the crack extended brick layer model can be seen. Since here in the model no corrections are considered the impedance for frequencies less than 10 Hz is higher than in reality. However, due to a crack damage, three time constants may appear in the impedance spectra under certain conditions as shown before.

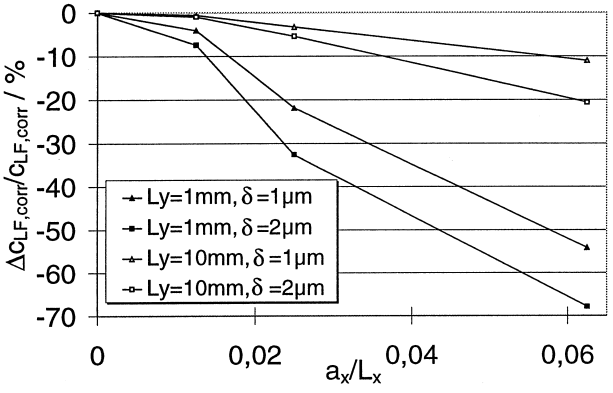

Fig. 19. Relative changes in capacitance depending on the related crack length a_x/L_x for two different crack openings and sample thicknesses calculated with the corrected, crack extended brick layer model.

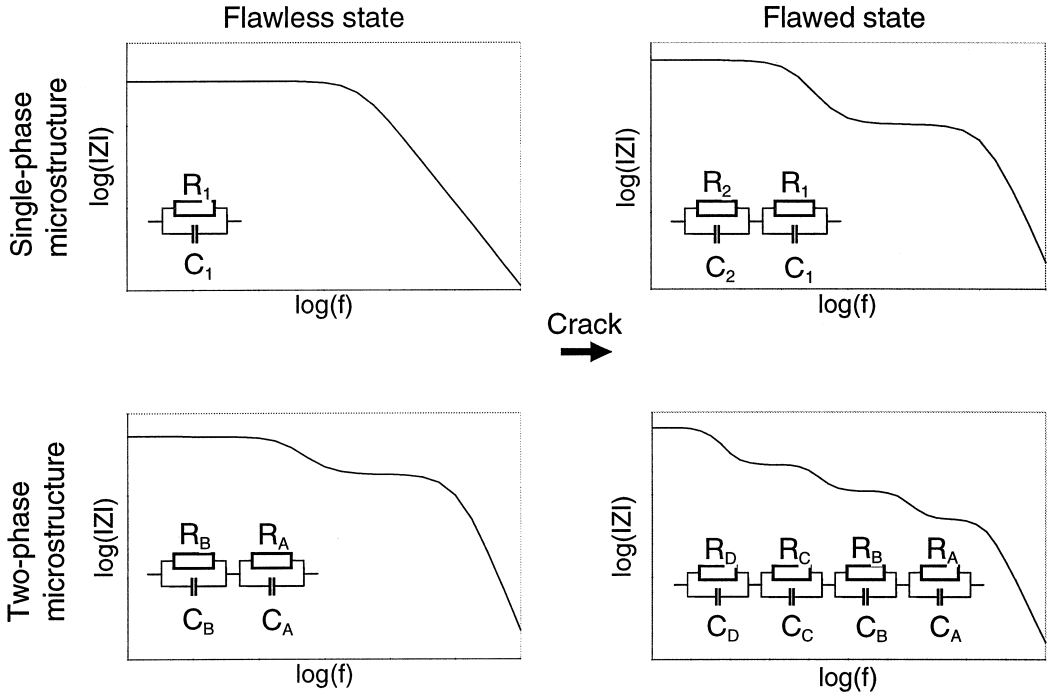

Fig. 20. Maximally possible number of distinguishable electrical time constants in the impedance spectra and corresponding equivalent circuits due to a crack damage for one- and two-phase microstructures.

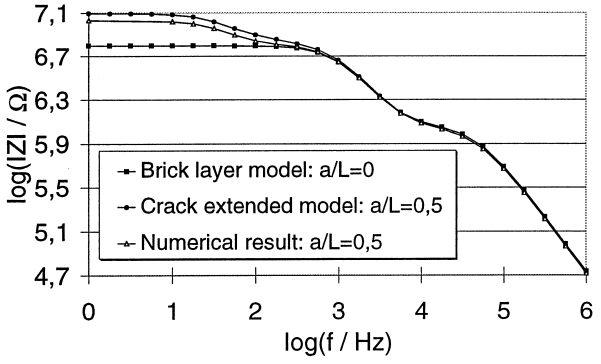

Fig. 21. Comparison of the impedance spectra of a fictitious material with a crack and without crack resulting from the numerical computations of the quasi static electrical field and from the crack extended brick layer model.

6. Conclusions

By means of impedance measurements on zirconia ceramics at elevated temperatures, one registers the ionic conductivity as well as the displacement current of the individual elements and phases of the microstructure. In particular, the partial impedances of the grains, of the grain boundary phase as well as of the crack have an effect in specific frequency ranges of the impedance spectra at temperatures above 250°C.

The crack damage only occurs in the low-frequency range of the spectra as a raised impedance which increases with increasing crack length. In the case of 9Ce- and 2Y-TZP there are no changes in the characteristics due to a crack damage in qualitative respect. The electrical behaviour can be still described by two time constants. In contrast to this in the spectra of 8YSZ clearly results an additional time constant due to a crack.

It succeeded to describe the electrical behaviour of flawed zirconia ceramics by means of the crack extended models qualitatively as it was found in the experiments. These two models which contain many single elements could be simplified by analytical transformations in each case in the form of a network consisting of two R-C elements in series. In the case of the crack extended brick layer model the electrical behaviour is described in general by four time constants. Therefore, a crack damage may result in a doubling of the existing time constants in the initial, flawless state as it was found for the single-phase 8YSZ materials. At least a third time constant may appear in the spectra if the volume fraction of the grain boundary phase is not small compared to the volume of the sample. In almost all real cases of two-phase microstructures, however, the impedance spectra are characterized by two time constants before and after cracking because of the geometrical conditions in the microstructure as well as of the assumed low-conducting grain boundary phase. The influence of a crack with its length and its opening clearly follows from the quantities of the R-C element which appear in the low-frequency range of the spectra. By means of the numerical computations of the static electrical fields the

deviations in the crack extended models resulting from the assumption of one-dimensional current flow can almost completely be corrected. Using the corrected, crack extended models, one finds an high agreement with the experimental results not only qualitatively but also quantitatively with an error limit of 5%.

With the capacitance and the resistance of the R-C element which appear in the low-frequency range of the spectra there exist two quantities, which both react considerably more sensitive to a crack damage than the effective total permittivity at room temperature as well as the total dc conductivity. For crack openings bigger than 1 μm, one finds the highest sensitiveness with the change in capacitance. Since the change in conductivity does not depend on the crack opening with the resistance there is always a second very sensitive quantity in the case of small crack openings. The calculated relative changes of both quantities correspond very well with the changes experimentally determined. With the corrected, crack extended models, therefore, the changes of the electrical impedance due to a crack damage can be predicted for any crack length and opening. The measuring sensitiveness always depends on the sample geometry as well as on the arrangement of the electrodes. With the given measuring accuracy of 0.2% for instance a crack of a length of less than 10 μm in a sample of the size $1\times8\times12$ mm^3 should be detectable.

In addition, the model calculations using the corrected, crack extended models can be transmitted to all polycrystalline materials for which in the flawless initial state the brick or the brick layer model is valid.

Acknowledgements

This work was funded by "Deutsche Forschungsgemeinschaft (DFG)" under the contract No. Ho 693/11 and Ob 104/4. We would also like to thank to Mrs. Wagner for the preparation and the microstructural characterization of the samples.

References

1. El Barhmi, A., Schouler, E. J., Hammou, A. and Kleitz, M., Electrical properties of tetragonal partially stabilized zirconia. In *Advances in Ceramics*, Vol. 24B. Am. Ceram. Soc., 1988, pp. 885–894.
2. Bauerle, J. E., Study of solid electrolyte polarisation by a complex admittance method. *J. Phys. Chem. Solids*, 1969, **30**, 2657–2670.
3. Kleitz, M., Bernard, H., Fernandez, E. and Schouler, E., Impedance spectroscopy and electrical resistance measurements on stabilized zirconia. In *Advances in Ceramics*, Vol. 3. Am. Ceram. Soc., 1981, pp. 310–336.
4. Muccillo, E. N. and Kleitz, M., Impedance spectroscopy of Mg-partially stabilized zirconia and cubic phase decomposition. *J. Eur. Ceram. Soc.*, 1996, **16**, 453–465.
5. Magistris, A. and Chiodelli, G., The dielectric response of zirconia-based materials. In *Advances in Ceramics*, Vol. 24B. Am. Ceram. Soc., 1988, pp. 895–900.
6. Beekmans, N. M. and Heyne, L., Correlation between impedance, microstructure and composition of calcia-stabilized zirconia. *Electrochim. Acta*, 1976, **21**, 303–310.
7. van Dijk, T. and Burggraaf, A. J., Grain boundary effects on ionic conductivity in ceramic $Gd_xZr_{1-x}O_{2-(x/2)}$ solid solutions. *Phys. Stat. Sol. (a)*, 1981, **63**, 229–240.
8. Verkerk, M. J., Middlehuis, B. J. and Burggraaf, A. J., Effect of grain boundaries on the conductivity of high-purity zirconium oxide–yttrium oxide ceramics. *Solid State Ionics*, 1982, **6**, 159–170.
9. Schouler, E. J., *Etude des Cellules a Oxyde Electrolyte par la Methode des Impedances Complexes*. PhD Thesis, Institut National Polytechnique de Grenoble, 1979.
10. Dessemond, L. and Kleitz, M., Effects of mechanical damage on the electrical properties of zirconia ceramics. *J. Eur. Ceram. Soc.*, 1992, **9**, 35–39.
11. Kleitz, M., Pescher, C. and Dessemond, L., Impedance spectroscopy of microstructure defects and crack characterization. In *Science and Technology of Zirconia V*. Australasian Ceram. Soc., 1993, pp. 593–608.
12. Tiefenbach, A., *Elektrische Charakterisierung mechanischer Schädigungen in ZrO_2-Keramik*. VDI:-Fortschrittsberichte 5/555. VDI-Verlag, Düsseldorf, 1999.
13. Abell, M. L. and Braselton, J. P., *The Maple V Handbook*. Academic Press, London, 1994.
14. Anon., *MAFIA Software Dokumentation*. Gesellschaft für Computersimulationstechnik, Darmstadt, 1997.
15. Anon, *Maxwell Software Dokumentation*. Ansoft Corporation, Pittsburgh, 1995.
16. Steil, M. C., Thevenot, F. and Kleitz, M., Densification of yttria-stabilized zirconia: Impedance spectroscopy analysis. *J. Electrochem. Soc.*, 1997, **144**(1), 390–398.